HERMITIAN COMPACT INTERPOLATION ON THE CUBED-SPHERE GRID

JEAN-PIERRE CROISILLE †‡

Abstract. The cubed-sphere grid is a spherical grid made of six quasi-cartesian square-like patches. It was originally introduced in [21]. We extend to this grid the design of high-order finite-difference compact operators [4, 11]. The present work is limitated to the design of a fourth-order accurate spherical gradient. The treatment at the interface of the six patches relies on a specific interpolation system which is based on using great circles in an essential way. The main interest of the approach is a fully symmetric treatment of the sphere. We numerically demonstrate the accuracy of the approximate gradient on several test problems, including the cosine-bell test-case of Williamson *et al.* [27] and a deformational test-case reported in [13].

Keywords: cubed-sphere grid - finite difference scheme - Hermitian compact perator - Spherical Harmonics.

1. Introduction

Representing discrete data on the surface of a sphere is an important topic for the numerical simulation of many problems in physics. Several spherical grids have been investigated, the most classical being the longitude-latitude grid, which is particularly famous in climatology. Here we focus on the cubed-sphere grid, originally introduced in [21].

Recently this grid regained interest for numerical simulations [19]. It is now widely used for different applications. In climatology it is used with various kinds of spatial approximation of the shallow-water system on the rotating earth. For example in [20, 16, 26] the finite-volume method is used (one unknown by cell). In [25] the cubed-sphere is used with the Spectral-Element method. In [14, 12, 10] the Discontinuous Galerkin approach is preferred. The cubed-sphere is also used for other applications. An analysis of the earth gravitational field is performed in [8]. In cosmology, black holes dynamics is studied in [5].

In this paper we focus on calculating a high-order accurate approximate gradient on the cubed-sphere. Specifically suppose given pointwise values of a grid function on the cubed-sphere, then we want to evaluate a high-order approximation to the spherical gradient (in the finite difference sense) at the same grid points. The main properties of our discrete gradient are:

- The data are supposed to be classical "finite-difference" values $u_{i,j}$ located on the six faces of the cubed-sphere.
- We take advantage of the fact that the coordinate lines of the cubed-sphere are sections of great circles. The first step of the algorithm consists in calculating finite difference hermitian derivatives along these great circles.
- In a second step an approximate value of the spherical gradient is deduced on each patch of the cubed-sphere. It is numerically observed to be uniformly fourth-order accurate.

Date: Feb 23, 2013.

This work was made during a sabbatical year at the C.N.R.S. (Centre National de la Recherche Scientifique, France). The author thanks N. Paldor for his support and encouragement. This work also beneficiated from helpful discussions with M. Ben-Artzi, F. Bouchut and T. Dubos.

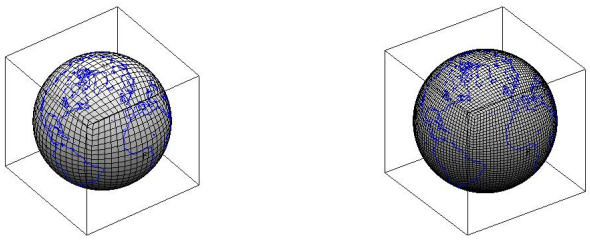

FIGURE 1. The cubed-sphere grid with $N = 16$ (left) and $N = 32$ (right).

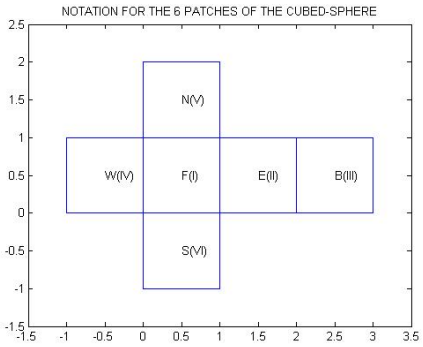

FIGURE 2. Topology of the six patches of the cubed-sphere grid. The number (I), (II), (III), (IV), (V), (VI) correspond to the faces *Front* (F), *East*(E), *Back* (B), *West* (W), *North* (N) and *South* (S).

The outline of the paper is as follows. In Section 2, we briefly recall the two main ingredients of the study: the geometric setting of the cubed-sphere grid and the hermitian derivative of a grid function. Section 3 is devoted to our interpolation procedure to define a uniformly fourth-order discrete spherical gradient on the cubed-sphere. Finally in Section 4 we numerically demonstrate the practical accuracy of our approximate gradient on several test-cases. First we show on two spherical advective test-cases [27, 13] that a centered scheme gives accurate and stable results, in a similar fashion to wave problems in aeroacoustics [24, 6, 3]. Second we show how to deduce an approximation to the spherical Laplacian and this approximation is further used on a discrete eigenvalue problem.

2. Background on the cubed-sphere grid and hermitian derivatives

Two main ingredients are used in the sequel. First in Section 2.1 we recall some geometric background useful to define the cubed-sphere. Then in Section 2.2 the principle of calculation of fourth-order hermitian derivatives on an irregular one-dimensional grid is described.

2.1. The cubed-sphere grid.

We consider a sphere of radius 1 centered at the origin O inscribed in the cube with same center and edge length 2. The reference cartesian frame is $(O, \boldsymbol{i}, \boldsymbol{j}, \boldsymbol{k})$. The directions of the unit vectors $\boldsymbol{i}, \boldsymbol{j}$ and $\boldsymbol{k}$ are associated with directions *Front*, *East* and *North*, respectively [19]. The cubed-sphere grid is made of six identical patches, denoted by *Front (I)*, *East (II)*, *Back (III)*, *West (IV)*, *North (V)*, and *South (VI)*, (Fig.2). The notation of the patches is indifferently:

the full name, letter notation *F, B, E, W, N, S* or number notation *I, II, III, IV, V, VI*. A natural reference frame on each patch is the *equiangular coordinate system*. It consists into the *equatorial* angle ξ and the *latitudinal* angle η with origin at the center of the patch. We thus have six coordinate systems denoted by

$$(\xi^F,\eta^F),\quad (\xi^B,\eta^B),\quad (\xi^E,\eta^E),\quad (\xi^W,\eta^W),\quad (\xi^N,\eta^N),\quad (\xi^S,\eta^S). \tag{1}$$

We simply note (ξ,η) whenever there is no ambiguity. The angles (ξ,η) are such that

$$-\frac{\pi}{4}\le \xi,\eta \le \frac{\pi}{4}. \tag{2}$$

Let N be the size parameter of the discretization. We consider on each patch a regular cartesian grid in the local (ξ,η) system

$$(\xi = i\Delta\xi, \eta_j = j\Delta\eta),\ \ -M = -N/2 \le i,j \le M = N/2 \tag{3}$$

The parameters $\Delta\xi$, $\Delta\eta$ are defined by

$$\Delta\xi = \frac{\pi}{2N},\quad \Delta\eta = \frac{\pi}{2N}. \tag{4}$$

The *cubed-sphere grid* is then obtained by mapping onto the sphere each point of these six cartesian grids by the central projection of center O.

Each of the six patches on the cubed-sphere thus consists of N^2 cells having a squared shape. Summing up the number of points in the six patches gives $6(N+1)^2$ points. However $12(N-1)$ points are counted twice along the interfaces between the patches and 8 points are counted three times (the vertices of the cube), thus giving an effective grid size of $6N^2+2$ points.

Some analytical formulas useful to perform the change of variable are given in the Appendix in Section 6. See also [19, 10, 26].

2.2. **Hermitian derivatives in one dimension.** In this section we recall the principle of calculation of the hermitian gradient in one dimension.

Consider first the design of the fourth-order hermitian derivative on a regular grid of the interval $\bar\Omega = [0,1]$. The discrete points are denoted by $0 = t_0 < t_1 = h < t_2 = 2h < \dots t_{N-1} = (N-1)h < t_N = 1$. Suppose given periodic data u_j at t_j, $(u_N = u_0)$. The hermitian compact operator $j \mapsto u_{t,j}$ approximating $u'(t_j)$ is defined by the linear system

$$\frac{1}{6}u_{t,j-1} + \frac{2}{3}u_{t,j} + \frac{1}{6}u_{t,j+1} = \frac{u_{j+1}-u_{j-1}}{2h},\ \ \sigma_{N+j} = \sigma_j,\qquad 0\le j\le N-1. \tag{5}$$

The hermitian derivative $u_{t,j}$ is fourth-order accurate at t_j in the finite difference sense, with a truncation error

$$u_{t,j} = u'(t_j) - \frac{h^4}{180}u^{(5)}(t_j) + O(h^6),\ \ 0\le j\le N-1. \tag{6}$$

We refer to the classical references [4, 11], and to [1] for a detailed numerical analysis.

Consider now the case of an irregular periodic grid on $\Omega = [a,b]$ given by x_j, $0\le j\le N-1$. The values x_j are in increasing order. The function φ is selected such that $x_j = \varphi(t_j)$. The grid $t_j = j\Delta t$ is a regular discretisation of the reference interval $\bar\Omega = [0,1]$. The chain-rule at point t_j can be written as

$$u'(\varphi(t)) = \frac{(u\circ\varphi)'(t)}{\varphi'(t)},\quad 0<t<1. \tag{7}$$

According to (7) the hermitian derivative at x_j is defined by

$$\bar u_{x,j} = \frac{(u\circ\varphi)_{t,j}}{\varphi_{t,j}},\ \ 0\le j\le N-1. \tag{8}$$

where $\varphi_{t,j}$ (respectively $(u\circ\varphi)_{t,j}$) is the hermitian derivatives of $\varphi(t)$ (respectively $(u\circ\varphi)(t)$) at t_j. In the case where $\varphi(t)$ is the cubic spline interpolating the values x_j, then it is easily seen that $\varphi_{t,j}=\varphi'(t_j)$. Thus $(u\circ\varphi)_{t,j}$ and $\varphi_{t,j}$ are fourth-order accurate approximations of $(u\circ\varphi)'(t_j)$ and $x'(t_j)$, respectively. As a consequence, $\bar{u}_{x,j}$ is a fourth-order approximation of $u'(x_j)$.

The calculation proceeds as follows. Define the periodic matrices $P,K\in\mathbb{M}_N(\mathbb{R})$,

$$P=\begin{bmatrix} 4 & 1 & 0 & \dots & 1\\ 1 & 4 & 1 & \dots & 0\\ \vdots & \vdots & \vdots & \dots & \vdots\\ 0 & \dots & 1 & 4 & 1\\ 1 & \dots & 0 & 1 & 4 \end{bmatrix}. \tag{9}$$

and

$$K=\begin{bmatrix} 0 & 1 & 0 & \dots & -1\\ -1 & 0 & 1 & \dots & 0\\ \vdots & \vdots & \vdots & \dots & \vdots\\ 0 & \dots & -1 & 0 & 1\\ 1 & \dots & 0 & -1 & 0 \end{bmatrix}. \tag{10}$$

Let $[\boldsymbol{u}],[\boldsymbol{x}]\in\mathbb{R}^N$ be the vector data corresponding to $(u_j)_{0\le k\le N-1}$ and $(x_j)_{0\le j\le N-1}$, respectively. Then the vectors $[\boldsymbol{u}_x],[\boldsymbol{x}_t]\in\mathbb{R}^N$ are solutions of

$$P[\boldsymbol{u}_t]=3K[\boldsymbol{u}],\quad P[\boldsymbol{x}_t]=3K[\boldsymbol{x}]. \tag{11}$$

The vector of the hermitian derivative $[\bar{u}_x]$ is deduced componentwise by

$$\bar{u}_{x,j}=\frac{u_{t,j}}{x_{t,j}},\quad 0\le k\le N-1. \tag{12}$$

3. Hermitian gradient on the cubed-sphere

3.1. **Isocoordinate systems of great circles.** Our starting point in the observation that the coordinate lines $\eta=cste$, $\xi=cste$ of each patch are great circle sections. Consider first an iso-η line of patch *Front*. We call α the curvilinear absissa along this coordinate line with eastward orientation. The angle α is such that

$$-\alpha_0(\eta)<\alpha<\alpha_0(\eta),\quad \alpha_0(\eta)=\operatorname{atan}\left(\frac{\sqrt{2}\tan\eta}{2}\right). \tag{13}$$

As the angle α increases, the coordinate line extends to a full great circle going across the patches *East*, *Back*, and *West* in this order. Fig. 3 displays the four patches E,W,B,W in local (ξ,η) coordinates together with the great circle coordinate line $\eta^F=\eta_0^F$. On the *East* patch it crosses the grid along a set of points M_k with local coordinates $(\xi_k^E=k\Delta\xi,\eta_k^E)$, $0\le k\le N$. Then it matches on patch *Back* the coordinate line $\eta^B=\frac{\pi}{2}-\eta_0^F$. Again on the *West* patch it crosses the grid along a set of points with local coordinates $(\xi_k^W=k\Delta\xi,\eta_k^W)$, $0\le k\le N$.

In a similar fashion we consider all the great circles defined as iso-ξ coordinate lines of face *Front*. These great circles are parametrized by the angle β, which is the curvilinear abscissa along them.

The other five patches E,B,W,N,S are treated in the same way. However due to the aforementionned match between patches *Front/Back*, *East/West*, *North/South*, respectively, it turns out that six sets of such coordinate based great circles are sufficient to cover the cubed-sphere. We define these six sets as follows:

(1) The two sets (I_α) and (I_β) are based on patch *Front*. They are defined by the iso-η lines and iso-ξ lines, respectively. They match the iso-η lines and iso-ξ-lines on patch *Back*, respectively.

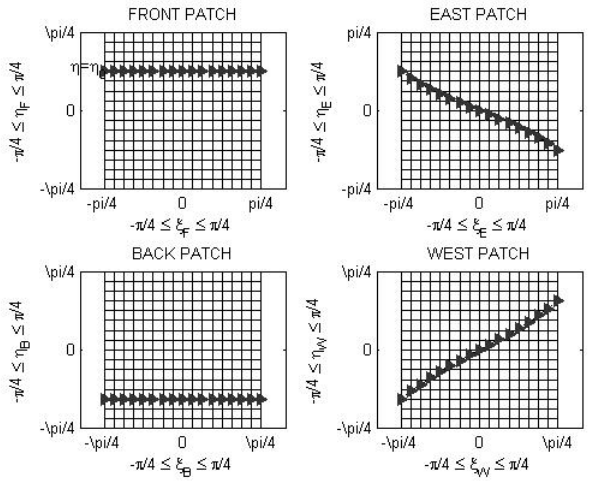

FIGURE 3. Representation of a great circle of the set (I_α). It coincides with the coordinate line $\eta = \eta_0$ of patch *Front* (top left). Then it crosses the patch *East* (top right) along a set of points (ξ_i^E, η_i^E). Then (bottom left) it coincides with the coordinate line $\eta = \pi - \eta_0$ on patch *Back*. Finally (bottom right) it crosses the patch *West*.

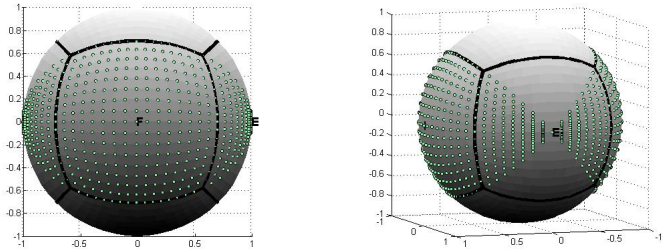

FIGURE 4. The set (I_α) of great circles corresponding to the iso-η coordinate lines of patch F. The great circles are plotted with the 'o' symbol. They all cross the *East* patch at the center point E. The displayed grid corresponds to $N = 16$ with 1538 points. Left: view of the Front Face. Right: view of the East Face.

(2) The two sets (II_α) and (II_β) are based on patch *East*. They are defined by the iso-η lines and iso-ξ lines, respectively. They match the iso-η lines and iso-ξ lines of patch *West*, respectively.
(3) The two sets (V_α) and (V_β) are based on patch *North*. They are defined by the iso-η lines and iso-ξ lines, respectively. They match the iso-η lines and iso-ξ lines of patch *South*, respectively.

The set (I_α) is represented on Fig. 4. As already mentionned we adopt as a generic notation α for the angle (curvilinear abscissa) for the circles of the sets (I_α), (II_α), (V_α). Similarly we call β the angle for the sets (I_β), (II_β), (V_β).

3.2. **Hermitian derivatives along great circles.** As explained above the coordinate lines of each of the six patches are sections of great circles. This property is the basis of the calculation of our approximate gradient at each grid point.

Suppose given data $u^k_{i,j}$, $-M \leq i,j \leq M$ at the coordinate points of each of the six patches $k = I, II, III, IV, V, VI$. The computation procedure of the high-order gradient can be summarized in the two following steps:

(1) Compute the Hermitian derivatives along the six sets of great circles (I_α), (I_β), (II_α), (II_β), (V_α), (V_β) according to formula (8) and (12).
(2) Deduce the gradient at each point of the six patches using an appropriate change of variables.

Concerning the first step we limit ourselves to describe how the hermitian derivative along the circles of the set (I_α) is approximated.

Consider a great circle C of the set (I_α). It corresponds to an isoline $\eta = \eta^F_0 = j_0\Delta\eta$. The values u^F_{i,j_0} are located along the great circle with the index i such that $-M \leq i \leq M$. Continuing eastward (see Fig. 3), the circle C crosses the patch *East*, on which data are interpolated as follows. The circle C crosses each iso-ξ^E lines $\xi^E = \xi^E_{i_0} = i_0\Delta\xi$ at a point with coordinates $(\xi^E_{i_0}, \beta_{i_0,j_0})$ in the (ξ^E, β) coordinate system of patch *East*. The value β_{i_0,j_0} is easily found as the solution of an intersection system we describe now. The coordinate system on the set (II_β) is (ξ^E, β). It is related to the cartesian coordinates (x, y, z) by

$$\left\{\begin{array}{l} x = -\cos\beta\sin\xi^E, \\ y = \cos\beta\cos\xi^E, \\ z = \sin\beta. \end{array}\right. \tag{14}$$

The intersection system bewteen the circle $\eta^F = \eta^F_{j_0}$ of the set (I_α) and the circle $\xi^E = \xi_{i_0}$ of the set (II_β) is the point with coordinate $(\xi^E_{i_0}, \beta_{i_0,j_0})$ where β_{i_0,j_0} is easily found to be (see Section 6),

$$\beta_{i_0,j_0} = \operatorname{atan}\left(-\sin\xi^E_{i_0}\tan\eta^F_{j_0}\right). \tag{15}$$

Since the point with coordinate $(\xi^E_{i_0}, \beta_{i_0,j_0})$ does not belong to the grid, we need an interpolated value of the grid function $u^k_{i,j}$ at it. We adopt a cubic spline interpolation in the variable β^E based on the grid values $u^{II}_{i_0,j}$, $-M \leq j \leq M$. The "not a knot" end condition is selected. The third section of the circle C coincides with the iso-η coordinate circle on the *Back* patch with coordinate number $-j_0$. As for the patch F the values $u^B_{i,-j_0}$, $-M \leq i \leq M$, belong to the data along the great circle C. Continuing eastward, the fourth section of the circle C goes across the *West* patch. Again a cubic spline interpolation as on the East patch is performed. As a final output we obtain a set of data along the circle C.

The periodic hermitian derivative operator (12) is applied to this set. The space variable is the angle $\alpha \in [0, 2\pi)$. This gives a set of approximate values of $\frac{\partial u(\alpha,\eta)}{\partial\alpha}_{|\eta}$ along the circle C. Restricting this set to patches $I(Front)$ and $III(Back)$ yields the approximations

$$\left\{\begin{array}{l} u^I_{\alpha,i,j} \simeq \left[\dfrac{\partial u(\alpha,\eta)}{\partial\alpha}_{|\eta}(\xi_i,\eta_j)\right]^I, \quad -M \leq i,j \leq M, \\ u^{III}_{\alpha,i,j} \simeq \left[\dfrac{\partial u(\alpha,\eta)}{\partial\alpha}_{|\eta}(\xi_i,\eta_j)\right]^{III}, \quad -M \leq i,j \leq M. \end{array}\right. \tag{16}$$

An analog procedure is used along each circle of the six sets (I_α), (I_β), (II_α), (II_β), (V_α) and (V_β). This finally provides approximate values of the two partial derivatives

$$\frac{\partial u(\alpha,\eta)}{\partial\alpha}_{|\eta}, \quad \frac{\partial u(\xi,\beta)}{\partial\beta}_{|\xi}, \tag{17}$$

along all the coordinate lines of each patch k, $I \leq k \leq VI$.

3.3. **Hermitian approximate spherical gradient.** We now consider the expression of the spherical gradient $\boldsymbol{\nabla}_s u$ at each point of the six patches of the cubed-sphere in the local (ξ,η) coordinate system:

$$\boldsymbol{\nabla}_s u = \frac{\partial u}{\partial \xi}_{|\eta} \boldsymbol{g}^{\xi} + \frac{\partial u}{\partial \eta}_{|\xi} \boldsymbol{g}^{\eta}. \tag{18}$$

where $(\boldsymbol{g}^{\xi},\boldsymbol{g}^{\eta})$ is the contravariant basis at point (ξ,η), see (66).

Having at hand approximate values of the partial derivatives $\frac{\partial u}{\partial \alpha}_{|\eta}$ and $\frac{\partial u}{\partial \beta}_{|\xi}$ in (16), we deduce by change of variables approximate values of $\frac{\partial u}{\partial \xi}_{|\eta}$ and $\frac{\partial u}{\partial \eta}_{|\xi}$, to be substituted into (18). We have

$$u(\xi,\eta) = u(\alpha(\xi,\eta),\eta) = u(\xi,\beta(\xi,\eta)), \tag{19}$$

so that the chain rule yields

$$\left\{ \begin{array}{l} \dfrac{\partial u}{\partial \xi}_{|\eta} = \dfrac{\partial u}{\partial \alpha}_{|\eta} \dfrac{\partial \alpha}{\partial \xi}_{|\eta}, \\ \dfrac{\partial u}{\partial \eta}_{|\xi} = \dfrac{\partial u}{\partial \beta}_{|\xi} \dfrac{\partial \beta}{\partial \eta}_{|\xi}. \end{array} \right. \tag{20}$$

In order to compute the two values $\frac{\partial \alpha}{\partial \xi}_{|\eta}$ and $\frac{\partial \beta}{\partial \eta}_{|\xi}$ we use the relations between the system of angles (ξ,η) and (α,β). It depends on the patch that is considered. Consider for example the *Front* patch (I). We have the two trigonometric identities (see Section 6),

$$\left\{ \begin{array}{l} \tan\alpha = \cos\eta \tan\xi, \\ \tan\beta = \cos\xi \tan\eta. \end{array} \right. \tag{21}$$

Using (18), (20), (21), we thus obtain that the spherical gradient at each point of the *Front* patch is deduced from $\frac{\partial u}{\partial \alpha}_{|\eta}$ and $\frac{\partial u}{\partial \beta}_{|\xi}$ by

$$\boldsymbol{\nabla}_s u = \frac{\partial u}{\partial \alpha}_{|\eta} \left(\cos\eta \frac{1+\tan^2\xi}{1+\cos^2\eta\tan^2\xi} \right) \boldsymbol{g}^{\xi} + \frac{\partial u}{\partial \beta}_{|\xi} \left(\cos\xi \frac{1+\tan^2\eta}{1+\cos^2\xi\tan^2\eta} \right) \boldsymbol{g}^{\eta}. \tag{22}$$

Our approximate spherical gradient is deduced from (22) replacing the derivatives $\frac{\partial u}{\partial \alpha}_{|\eta}$ and $\frac{\partial u}{\partial \beta}_{|\xi}$ by their hermitian approximations. On patch *Front (I)*, this gives the pointwise approximation

$$\begin{array}{rl} \boldsymbol{\nabla}_{s,h} u^I_{i,j} & = u^I_{\alpha,i,j} \left(\cos\eta_j \dfrac{1+\tan^2\xi_i}{1+\cos^2\eta_j\tan^2\xi_i} \right) \boldsymbol{g}^{\xi,I}_{i,j} \\ & + u^I_{\beta,i,j} \left(\cos\xi_i \dfrac{1+\tan^2\eta_j}{1+\cos^2\xi_i\tan^2\eta_j} \right) \boldsymbol{g}^{\eta,I}_{i,j}. \end{array} \tag{23}$$

Analog expressions hold for the five other patches.

3.4. **Interface and corner points.** *Interface points* correspond to the points of the cubed-sphere located along the 12 "edges" at the interface of the patches. Each of these point belongs to two patches. There are $12(N-1)$ such points. The *corner points* match the eight vertices of the inscribed cube. They are end points of the "edges" and each of them belongs to three patches. On a given patch the indices in (3) of the $4(N-1)$ interface points are

$$\left\{ \begin{array}{l} i = \pm M,\ -M+1 \le j \le M-1, \\ -M+1 \le i \le M-1,\ j = \pm M. \end{array} \right. \tag{24}$$

The four corner points are

$$(-M,-M),\ (-M,M),\ (M,-M),\ (M,M). \tag{25}$$

Consider for example an interface point $\boldsymbol{x}$ located on the boundary between the Front and the East patches. At this point, the preceding calculation procedure provides two formulas for $\boldsymbol{\nabla}_s u$, the first

one using the Front (I) coordinate system, the second one using the East (II) coordinate system. By symmetry, we adopt as a final formula at this point the half-sum of the two discrete gradients. Similarly the discrete gradient at one of the eight "corner" points $\boldsymbol{x}_c$ is obtained with a $1/3$ weighting of the approximations of gradients of the three patches where $\boldsymbol{x}_c$ is located.

3.5. **Summary and remarks.** The algorithm above to approximate the spherical gradient can be summarized as follows:

(i) Assemble the system of data along the six networks of great circles (I_α), (I_β), (II_α), (II_β), (V_α) and (V_β). Each great circle has four sections. The data along the first and third sections are copied from the primary data. The second and fourth sections require a cubic spline interpolation along each coordinate line orthogonal to the circle (in the (ξ, η) system).
(ii) Compute the periodic hermitian derivatives along each circle of the six networks.
(iii) Compute the spherical gradient on each patch using formulas like (23).

An essential aspect of this procedure is that the discrete (hermitian) derivative along the six sets of great circles approximates an *intrinsic* quantity (the derivative of the grid function with respect to the curvilinear abscissa). Using a change of variables to the local equiangular coordinates (ξ, η) in (23) to express the gradient is for convenience only; other local basis could be considered. This is in contrast to [19, 26] where the local system (ξ, η) is used to calculate approximations. In particular no *ghost points* or specific boundary interpolation scheme are introduced. The treatment of the interface of the patches is obained as a corollary of the great-circle approach. Note also that the hermitian formula (11) can be easily replaced by any higher-order derivative compact operator [11]. The algorithm and most of the coding remain the same. In addition the algorithm is highly parallel in nature. The computations in step *(i)* and *(ii)* are purely one-dimensional. The core of the solver consists only in solving tridiagonal linear systems of size $4N$. The global arithmetic complexity is easily found to be $O(N^2)$.

4. Numerical results

4.1. **Spherical gradient accuracy.** We report the accuracy of the approximate spherical gradient in (23) when applied to a function $u(x, y, z)$. The discrete data are the grid function

$$u^k_{i,j} = u(x^k_{i,j}, y^k_{i,j}, z^k_{i,j}),\ -M \le i, j \le M, \quad I \le k \le VI. \tag{26}$$

The error is

$$e_\infty = \max_{I\le k\le VI,\, -M\le i,j\le M,\, 1\le l\le 3} \left| [\boldsymbol{\nabla}^k_s(\xi_i, \eta_j)]_l - [\boldsymbol{\nabla}^k_{s,h} u(\xi_i, \eta_j)]_l \right|. \tag{27}$$

The maximum is taken on the three components $1 \le l \le 3$ of the gradient and on all the points of the cubed-sphere.

4.1.1. *First test-case.* We report in Table 1 the error obtained for the gradient of the oscillating function

$$u(x, y, z) = \sin(10\pi x)\sin(2\pi y)\sin(6\pi z), \tag{28}$$

restricted to the unit sphere. The fourth-order accuracy of the calculated gradient is observed.

4.1.2. *Second test-case.* The next test-case [23] consists in approximating the gradient of the function $u(x, y, z) = \exp(x) + \exp(y) + \exp(z)$ restricted to the unit sphere. The results, reported in Table 2 compare favourably with the ones in [23], where an approximation based on spherical harmonics combined with an icosahedral grid is used. Again the fourth-order accuracy is observed in this case.

	N=8	rate	N=16	rate	N=32	rate	N=64	rate	N=128
e_∞	23.475	2.99	2.949	4.61	0.121	4.07	7.205(-3)	3.91	4.774(-4)
$\Delta\xi$ in km	1250		625		312.5		156.25		78.12
Nb of grid points	386		1538		6146		24578		93306

TABLE 1. Convergence rate of the hermitian gradient of the function $u(x,y,z) = \sin(10\pi x)\sin(2\pi y)\sin(6\pi z)$ restricted to the unit sphere.

	N=8	rate	N=16	rate	N=32	rate	N=64	rate	N=128
e_∞	5.323(-4)	4.07	1.912(-5)	4.00	1.191(-6)	4.00	7.432(-8)	3.72	5.622(-9)
$\Delta\xi$ in km	1250		625		312.5		156.25		78.12
Nb of grid points	386		1538		6146		24578		93306

TABLE 2. Convergence rate of the hermitian gradient of the function $u(x,y,z) = \exp(x) + \exp(y) + \exp(z)$ restricted to the unit sphere.

4.2. **Cosine-bell advection test-case.** We consider the cosine-bell convection problem described as a first test-case in [27]. This problem serves as a preliminary test to evaluate the accuracy of numerical methods for the shallow water system in global climatology on the spherical earth. Reference results for this test-case are widely reported in the literature by various numerical schemes [16, 26, 2]. It consists in a cosine-bell propagating at constant spherical solid velocity. The exact solution is the unperturbed profile after one full rotation around the earth. The unknown is the height of the bell $h(\boldsymbol{x},t)$, solution of the convection equation

$$\left\{ \begin{array}{l} \partial_t h(\boldsymbol{x},t) + \boldsymbol{c}\cdot\boldsymbol{\nabla}_s h(\boldsymbol{x},t) = 0, \\ h(\boldsymbol{x},0) = h_0(\boldsymbol{x}). \end{array} \right. \tag{29}$$

In the spherical longitude-latitude coordinate system (λ,θ), $0 \le \lambda < 2\pi$ and $-\pi/2 \le \theta \le \pi/2$. The tangent unit vectors $\boldsymbol{e}_\lambda, \boldsymbol{e}_\theta$ are

$$\left\{ \begin{array}{l} \boldsymbol{e}_\lambda = -(\sin\lambda)\boldsymbol{i} + (\cos\lambda)\boldsymbol{j}, \\ \boldsymbol{e}_\theta = -(\sin\theta\cos\lambda)\boldsymbol{i} - (\sin\theta\sin\lambda)\boldsymbol{j} + (\cos\theta)\boldsymbol{k}. \end{array} \right. \tag{30}$$

The solid body advective field is $\boldsymbol{c} = \boldsymbol{c}(\boldsymbol{x}) = u\boldsymbol{e}_\lambda + v\boldsymbol{e}_\theta$ with $u(\boldsymbol{x})$ and $v(\boldsymbol{x})$ expressed in the (λ,θ) coordinate system as

$$\left\{ \begin{array}{l} u = u_0(\cos\theta\cos\alpha + \sin\theta\cos\lambda\sin\alpha), \\ v = -u_0(\sin\lambda\sin\alpha). \end{array} \right. \tag{31}$$

The angle $\alpha \in [0, \pi/2[$ [1] is the angle of the plane motion with the $\boldsymbol{k}$ axis of the poles. The initial cosine-bell is

$$h_0(\lambda,\theta) = \left\{ \begin{array}{l} (h_0/2)\left(1 + \cos(\pi r(\theta,\lambda)/R)\right), \quad r(\theta,\lambda) < R, \\ 0, \ r \ge R. \end{array} \right. \tag{32}$$

The value $r(\lambda,\theta)$ is the great circle distance between (λ,θ) and the center of the cosine bell, initially taken at $(\lambda_c,\theta_c) = (3\pi/2, 0)$. It is given by [27]

$$r(\lambda,\theta) = a\arccos\left(\sin(\theta_c)\sin(\theta) + \cos(\theta_c)\cos(\theta)\cos(\lambda-\lambda_c)\right) \tag{33}$$

The numerical values associated with (30), (31), (32) are $a = 6.37122\,10^6 m$ (earth radius), $R = a/3$, $u_0 = 2\pi a/(12\,\text{days})$, and $h_0 = 1000m$.

[1] The angle α should not be confused with the curvilinear absissa introduced in Section 3.1.

The semi-discrete approximation we consider is the centered finite-difference scheme (method of lines) defined by

$$\frac{dh^k_{i,j}(t)}{dt} + \boldsymbol{c}_{i,j} \cdot \boldsymbol{\nabla}_{s,h} h^k_{i,j}(t) = 0, \quad -M \leq i,j \leq M, \quad I \leq k \leq VI, \tag{34}$$

where the approximate gradient $\boldsymbol{\nabla}_{s,h}$ is given in (23). The time-stepping scheme is the fourth-order Runge-Kutta (RK4) scheme. The CFL number is defined by

$$\mathrm{CFL} = u_0 \frac{\Delta t}{\Delta \xi}. \tag{35}$$

The scheme is observed to be stable with a time-step given by CFL = 1. To reduce the dispersive effects a filter of order 10 is applied at each time step along the great circles of the six networks considered in Section 3.1. The purpose is to add some dissipation to cancel high-frequency dispersive effects. Such a filtering is a common practice when using compact schemes for wave propagation problemes, e.g. in aeroacoustics [24, 6, 3]. For a one-dimensional gridfunction $(u_j)_{j\in\mathbb{Z}}$ the filter is the linear operator $(u_j)_{j\in\mathbb{Z}} \mapsto (u_{F,j})_{j\in\mathbb{Z}}$ defined by

$$u_{F,j} = \sum_k f_k u_{j+k}, \tag{36}$$

where the coefficients f_k are given by [17],

$$\begin{pmatrix} f_0 \\ f_1 = f_{-1} \\ f_2 = f_{-2} \\ f_3 = f_{-3} \\ f_4 = f_{-4} \\ f_5 = f_{-5} \end{pmatrix} = \begin{pmatrix} 772/1024 \\ 210/1024 \\ -120/1024 \\ 45/1024 \\ -10/1024 \\ 1/1024 \end{pmatrix}. \tag{37}$$

Note that the filter is applied only at each time-step and not at each internal step of the time scheme. Fig. 5 reports the history of the error using a discretisation with $N = 40$ (9602 unknowns) fand 160 time iterations with an angle $\alpha = 45^{\mathrm{deg}}$. The time step is $\Delta t = 6480s\,(108')$. Table 3 reports the value of the relative errors I_1, I_2, I_∞ as required in [27]. The error I_p is defined by

$$I_p = \frac{\|e\|_p}{\|h_{\mathrm{ex}}\|_p}, \quad 1 \leq p \leq +\infty, \tag{38}$$

where $e = h_{\mathrm{ex}} - h_{\mathrm{cal}}$ is the difference between the exact and the calculated solution. The notation $\|\,.\,\|_p$ stands for the canonical discrete version of the continuous functional norm with same name on the sphere, see (70), (71). The relative maximum and minimum errors are [26],

$$M(h) = \frac{\max h_{\mathrm{ex}} - \max h_{\mathrm{cal}}}{\max |h_{\mathrm{ex}}|}, \quad m(h) = \frac{\min h_{\mathrm{ex}} - \min h_{\mathrm{cal}}}{\max |h_{\mathrm{ex}}|}. \tag{39}$$

Finally we plot on Fig.6 the isolines of the calculated solution and of the difference between the calculated solution and the exact one for the case $\alpha = \pi/4$ (propagation towards north-east). Results on Fig.5 and Fig.6 compare favourably with analog results using schemes of same order. See for example [26] where a MUSCL finite-volume scheme combined with a fourth-order reconstruction procedure is used on a cubed-sphere of same size.

4.3. **A deformational test-case.** A deformational flow test-case consists in calculating the evolution of an initial data which undergoes a severe deformation during a linear advection transport phase. The analytic solution is not known during the transient but the solution returns to the initial state after some time period T. The accuracy of the scheme is thus measured at time $t = T$. The maximal deformation occurs at time $t = T/2$. Such a test-case offers an additional challenge compared to the

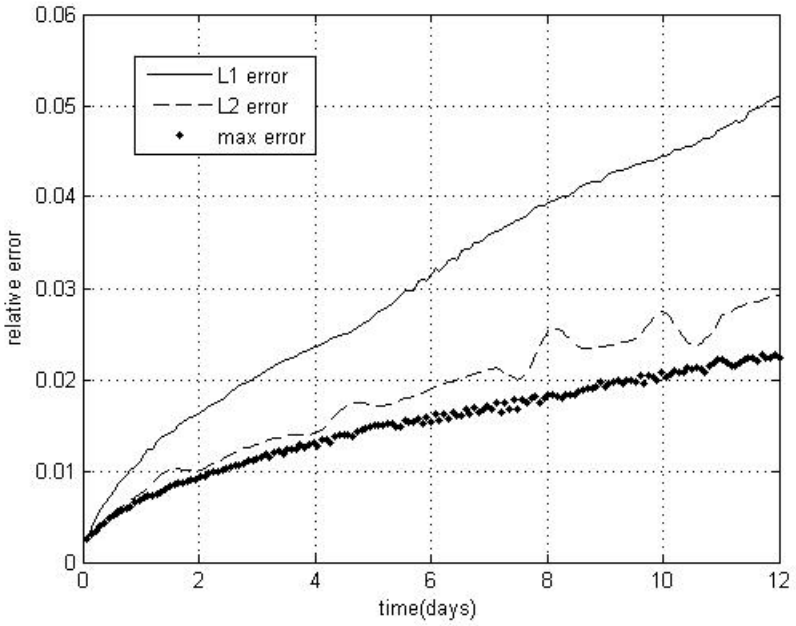

FIGURE 5. History of the three relative errors L^1, L^2, L^∞ for the cosine-bell advection test-case (29) for a cubed-sphere grid of size $N = 40$ and $\alpha = 45^{\text{deg}}$.

CFL	Direction	L_1 error	L_2 error	L_∞ error	M(h)	m(h)
1.0	$\alpha = 0^{\text{deg}}$	5.43601(-2)	3.26394(-2)	2.65404(-2)	2.50503(-2)	-2.65404(-2)
	$\alpha = 45^{\text{deg}}$	5.11205(-2)	2.93375(-2)	2.24284(-2)	2.11063(-2)	-2.24284(-2)
0.5	$\alpha = 0^{\text{deg}}$	4.0020(-2)	2.25259(-2)	1.91928(-2)	2.87524(-2)	1.91193(-2)
	$\alpha = 45^{\text{deg}}$	3.45757(-2)	1.86116(-2)	1.43016(-2)	1.27016(-2)	-1.43016(-2)

TABLE 3. Relative error for the cosine-bell advection test-case (29) with the fourth-order centered hermitian scheme (34) and the RK4 time-stepping scheme. The mesh size is $6 \times 40^2 + 2$ (9602 unknowns).

solid rotation test-case in Section 4.2. An example of deformational test is given [13] by the following linear convection equation with velocity $\boldsymbol{c}(\boldsymbol{x}, t)$

$$\begin{cases} \partial_t h(\boldsymbol{x}, t) + \boldsymbol{c}(\boldsymbol{x}, t) \cdot \boldsymbol{\nabla}_s h(\boldsymbol{x}, t) = 0, \\ h(\boldsymbol{x}, 0) = h_0(\boldsymbol{x}). \end{cases} \tag{40}$$

The divergence-free velocity $\boldsymbol{c}(\boldsymbol{x}, t) = \boldsymbol{\nabla}_s^\perp \psi(\boldsymbol{x}, t)$ is derived from the stream function $\psi(\boldsymbol{x}, t)$ by

$$\psi(\boldsymbol{x}, t) = k \sin^2(\lambda/2) \cos^2(\theta) \cos(\pi t/T), \quad k > 0, \tag{41}$$

The components u and v of $\boldsymbol{c}(\boldsymbol{x}, t)$ in the basis $(\boldsymbol{e}_\lambda, \boldsymbol{e}_\theta)$ are, see (30),

$$\begin{cases} u(\boldsymbol{x}, t) = -\psi_\theta = k \sin^2(\lambda/2) \sin(2\theta) \cos(\pi t/T) \\ v(\boldsymbol{x}, t) = \psi_\lambda / \cos\theta = (k/2) \sin(\lambda) \cos(\theta) \cos(\pi t/T). \end{cases} \tag{42}$$

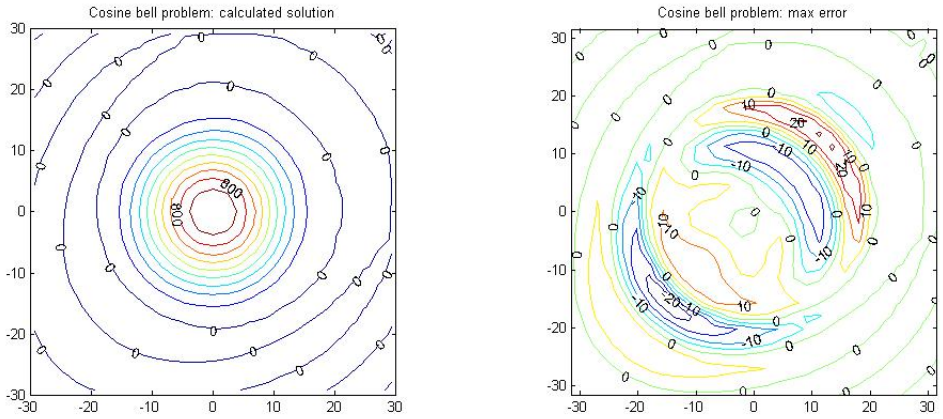

FIGURE 6. Contours after one rotation with $\alpha = \pi/4$. Left: numerical solution. Right: error. The cubed-sphere grid uses $N = 40$. The propagation is oriented towards north-east.

The initial condition is the double cosine-bell defined by

$$h_0(\lambda,\theta) = \begin{cases} (h_{\max}/2)\,(1+\cos(\pi r_i(\theta,\lambda)/R))\,, \; r_i(\theta,\lambda) < R, \\ 0, \; r \geq R, \;\; i = 1,2. \end{cases} \tag{43}$$

and $r_i(\lambda,\theta) = \arccos\left(\sin\theta_i \sin\theta + \cos\theta_i \cos\theta \cos(\lambda - \lambda_i)\right)$ is the great circle distance between (λ,θ) and(λ_i,θ_i) on the sphere of radius $a = 1$. The numerical scheme is fully centered with design given in (34). It is formally fourth-order in space and time. The tenth order filter (37) applied at each time step.

In Table 4 we report the numerical quantities I_α, $\alpha = 1, 2, \infty$ and the indicators at time T defined by [13]

$$M'(h) = \frac{\max h_{\rm cal} - \max h_{\rm ex}}{\Delta h_0}, \; m'(h) = \frac{\min h_{\rm cal} - \min h_{\rm ex}}{\Delta h_0}, \; \Delta h_0 = \max h_0 - \min h_0. \tag{44}$$

The parameters of the calculation are $T = 5$ (final time in (41)), $k = 2.4$ (strength of the stream-function (41)), $(\lambda_1,\theta_1) = (\pi,\pi/3)$, $(\lambda_2,\theta_2) = (\pi,-\pi/3)$ (location of the two initial cosine-bells (43)). Three grid sizes $N = 20$, $N = 40$, $N = 60$ are used. They correspond to a longitudinal angle discretisation of $4.5^{\rm deg}$, $2.25^{\rm deg}$, $1.5^{\rm deg}$, respectively. We report in Table 4 the results at time $t = T$ with grid size $N = 20$ (2402 unknowns), $N = 40$ (9602 unknowns), and $N = 60$, (21602 unknowns). The calculations are performed using 200, 400, 600 time steps, respectively, which corresponds to an approximate CFL number of 0.75.

With the finest grid ($N = 60$, 21602 unknowns), the error levels reported in Table 4 are of same order than the ones reported in [13] where a Discontinuous Galerkin method was used using 38400 unknowns and 2400 time steps. On Fig. 7 are reported the initial cosine bells (43), the solution at time $t = T/2$, the calculated final state at time $t = T$ where the two cosine bells return to their inital positions, and finally the error $h_{\rm cal} - h_{\rm ex}$ at time $t = T$.

N	Nb. of time steps	L_1 error	L_2 error	L_∞ error	$M'(h)$	$m'(h)$
20	160	0.1688	0.2666	0.2643	-0.2030	0.2627
40	320	0.0378	0.0636	0.0785	0.0006	-0.0591
60	640	0.0084	0.0154	0.0255	0.0007	-0.0213

TABLE 4. Relative error for the non divergent flow test-case (40) with the fourth-order centered hermitian scheme (34) combined with the RK4 time-stepping scheme. The grid $N = 60$ has 21602 ($=6\times60^2+2$) degrees of freedom, with a spatial resolution of 1.5^{deg} along the equator. The CFL number is approximately 0.75.

Again the results demonstrate the accuracy of the discrete spherical gradient operator (23) and the capabilities of the centered scheme (34) with filtering (37) compared to high-order conservative methods [13] on the sphere.

4.4. **A spherical Laplacian test-case using Spherical Harmonics.**

4.4.1. *Discrete approximate spherical Laplacian.* In this section we show how to deduce from the discrete spherical gradient (23) a simple formula to approximate the spherical laplacian at each point of the cubed-sphere. The spherical laplacian is defined by

$$\Delta_s u = \nabla_s \cdot (\boldsymbol{\nabla}_s u), \tag{45}$$

where $\nabla_s\cdot$ and $\boldsymbol{\nabla}_s$ are the spherical divergence and the spherical gradient, respectively. In the coordinate system (ξ,η) of the cubed-sphere, the spherical divergence operator of the vector field $\boldsymbol{F}$ is expressed as

$$\nabla_s \cdot \boldsymbol{F} = \frac{1}{\sqrt{\bar{G}}}\left(\frac{\partial}{\partial\xi}(\sqrt{\bar{G}}\boldsymbol{F}\cdot g^\xi) + \frac{\partial}{\partial\eta}(\sqrt{\bar{G}}\boldsymbol{F}\cdot g^\eta)\right). \tag{46}$$

where $\bar{G} = \sqrt{|\det G|}$ is the metric term and G is the covariant metric tensor (see (65)). From the gradient $\boldsymbol{\nabla}_s u$, we deduce on each patch the grid functions $u_1(\xi,\eta)$ and $u_2(\xi,\eta)$,

$$u_1(\xi,\eta) = \sqrt{\bar{G}}\boldsymbol{\nabla}_s u\cdot g^\xi, \quad u_2(\xi,\eta) = \sqrt{\bar{G}}\boldsymbol{\nabla}_s u\cdot g^\eta. \tag{47}$$

Using the discrete gradient (23) we obtain a discrete approximation of u_1 and u_2 as

$$(u_{1,h})^k_{i,j} = \sqrt{\bar{G}}\boldsymbol{\nabla}_{s,h}u^k_{i,j}\cdot g^\xi_{i,j}, \quad (u_{2,h})^k_{i,j} = \sqrt{\bar{G}}\boldsymbol{\nabla}_{s,h}u^k_{i,j}\cdot g^\eta_{i,j}. \tag{48}$$

Applying the fourth-order hermitian derivatives to $(u_{1,h})^k_{i,j}$, and $(u_{2,h})^k_{i,j}$ yields the approximate spherical Laplacian

$$\Delta_{s,h}u^k_{i,j} = \frac{1}{\sqrt{\bar{G}}}\left((u_{1,h})^k_{\xi,i,j} + (u_{2,h})^k_{\eta,i,j}\right). \tag{49}$$

In (49) $(u_{1,h})_\xi$ and $(u_{2,h})_\eta$ stand for the hermitian derivatives using (5), calculated on each patch. Using this setting boundary conditions for $(u_{1,h})_\xi$ and for $(u_{2,h})_\eta$ are needed in order for (5) to be applied at internal points. Here we adopt in the ξ and η directions the one-sided fourth-order approximate derivative given by [7],

$$u'(x) = \delta^+_x u_j - \frac{1}{2}(\delta^+_x)^2 u_j + \frac{1}{3}(\delta^+_x)^3 u_j - \frac{1}{4}(\delta^+_x)^4 u_j + O(h^4), \tag{50}$$

where at point x_j the forward difference operator δ^+_x is

$$\delta^+_x u_j = \frac{u_{j+1}-u_j}{h}. \tag{51}$$

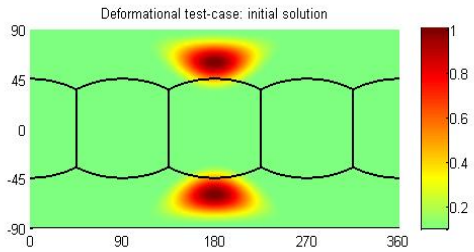

(a) Initial condition at $t = 0$

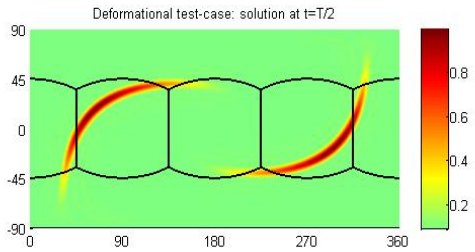

(b) Solution at $t = T/2$

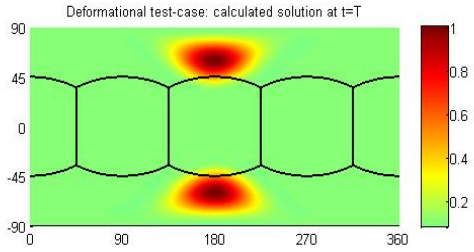

(c) Final position at $t = T$

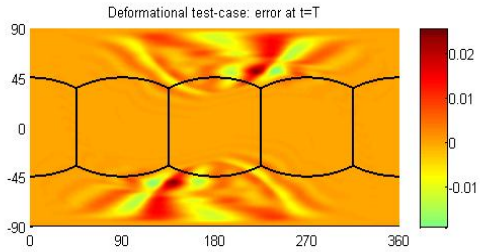

(d) error $h_{\text{cal}} - h_{\text{ex}}$ at $t = T$

FIGURE 7. Non divergent flow test-case (40). The final time is $T = 5$. The number of unknowns is 21602 for a resolution of 1.5^{deg} around the equator. The number of time-steps is 600 with an approximate CFL number of 0.75.

Formula (50) can be rewritten as the one-sided five-point operator

$$u_{x,i} = \frac{1}{12h}\left(-25u_i + 48u_{i+1} - 36u_{i+2} + 16u_{i+3} - 3u_{i+4}\right). \tag{52}$$

Finally we adopt at "edge" points and "corner" points the symmetric 1/2 and 1/3 averaging procedure of Section 3.4. This weighting is observed to retain the uniform fourth-order accuracy.

4.4.2. *A spherical eigenvalue test problem.* We demonstrate the numerical accuracy of the Laplacian (49) on the following problem. The spherical harmonic with index (n, m), $-n \le m \le n$, $0 \le n$ is the function defined in coordinates (θ, λ) by

$$f_n^m(\boldsymbol{x}) = \bar{P}_n^{|m|}(\sin\theta)e^{im\lambda}, \quad 0 \le \lambda < 2\pi, \quad -\pi/2 \le \theta \le \pi/2. \tag{53}$$

In (53) the function $\bar{P}_n^{|m|}(z)$ stands for the *associated Legendre polynomial* of order n, m with the standard normalization given by

$$\int_{-1}^{1} \bar{P}_n^{|m|}(x)^2 dx = 1. \tag{54}$$

We refer to [9] for a general reference on spherical harmonics. Here we adopt the notation of [18]. The main property of the spherical harmonics (53) is to be the eigenfunctions of the spherical Laplacian. The consistency relation for the spherical harmonics $f_m^n(\boldsymbol{x})$ that is numerically tested is

$$e(f_m^n) = \max_{-M \leq i,j \leq M, I \leq k \leq VI} |\,(\Delta_{h,s} f_m^n)_{i,j}^k - \lambda_n (f_m^n)_{i,j}^k|, \tag{55}$$

where the maximum is taken over all the points of the cubed-sphere. The eigenvalue λ_n is

$$\lambda_n = -n(n+1). \tag{56}$$

Table 5 reports the accuracy of (55) for the functions f_1^1, f_3^2, f_8^4, f_{14}^9 on a set of cubed-sphere grids. The results appear to be fourth-order accurate.

	N=8	rate	N=16	rate	N=32	rate	N=64	rate	N=128
$e(f_1^1)$	8.6508(-3)	3.74	6.4381(-4)	4.18	3.5512(-5)	4.34	1.7496(-6)	3.35	1.7066(-7)
$e(f_3^2)$	2.3477(-1)	3.70	1.8073(-2)	4.06	1.0805(-3)	3.68	8.3954(-5)	3.51	7.3302(-6)
$e(f_8^4)$	1.9702(1)	3.54	1.6991(0)	3.24	1.7884(-1)	3.98	1.1325(-2)	4.00	7.0537(-4)
$e(f_{14}^9)$	2.0246(2)	2.92	2.666(1)	3.06	3.1909	4.00	1.9809(-1)	3.96	1.2696(-2)
$\Delta\xi$ in km	1250		625		312.5		156.25		78.12
Nb of grid points	386		1538		6146		24578		93306

TABLE 5. Convergence rate of the error function $e(f_n^m)$ in (55) for several spherical harmonics functions.

5. Conclusion

This work demonstrates the efficiency and the accuracy of a new finite difference approximation method to the spherical gradient. It is based on the cubed-sphere grid and compact hermitian derivative along great circles. This allows to design centered compact schemes in a fashion similar to the planar case.

The present approach offers an interesting compromise with other high-order accurate approximation methods. In contrast to the longitude/latitude grid, it does not have the *pole problem*, yet keeping the idea of approximations along great circles. This is an important property when uniformly accurate approximations are required. In addition the degrees of freedom are *pointwise values* as in the standard finite-difference method. This is in contrast with collocation methods using a more elaborate analytical background based on special functions such as spherical harmonics [18] or spherical wavelets [22].

Applications to advanced mathematical climatology problems deserve further studies. A specific challenge consists in analyzing the conservativity properties of finite-difference schemes similar to (34). As in the non-spherical case it is a crucial issue for the numerical treatment of the shallow-water system on the sphere. Conservativity is by definition satisfied in *ab initio* conservative schemes such as finite-volume schemes [2, 26] or the Discontinuous Galerkin method [13]. However it turns out that wave problems on the sphere, (e.g. linearized versions of the SW system [15]), which are formulated in nonconservative form, are tractable using centered schemes similar to those presented in Sections 4.2 and 4.3.

Let us finally mention that a convergence analysis of the approximation procedure suggested in this work clearly deserves further attention.

6. Appendix: Cubed-sphere coordinate system and metrics

To perform the computation described in this paper we need several coordinate systems and the relation between them.

The cartesian reference frame is denoted by $(O, \boldsymbol{i}, \boldsymbol{j}, \boldsymbol{k})$, with origin O at the center of the sphere. The centers of the six patches I, II, III, IV, V, VI are the six points

$$F(1,0,0),\ B(-1,0,0),\ E(0,1,0),\ W(0,-1,0),\ N(0,0,1),\ S(0,0-1), \tag{57}$$

respectively.

Particularly useful are the *gnomonic coordinates* defined by

$$\begin{cases} X = \tan\xi, \\ Y = \tan\eta. \end{cases} \tag{58}$$

Using (X, Y) facilitates the actual coding of any computation using the cubed-sphere. For example, the cartesian coordinates of a grid point (x, y, z) of, say, the patch *Front*, are given in terms of the equiangular angles (ξ, η) by

$$\begin{cases} X = \frac{y}{x}, \\ Y = \frac{z}{x}, \\ x^2 + y^2 + z^2 = 1. \end{cases} \tag{59}$$

On each patch, we use in Section 3 the coordinate system (α, η) and (ξ, β). For the patch *Front*, the two systems are related by expressing the cartesian coordinates in terms of either (α, η) or (ξ, β) by

$$\begin{cases} x = \cos\alpha\cos\eta = \cos\beta\cos(-\xi), \\ y = \sin\alpha = -\cos(\beta)\sin(-\xi), \\ z = \cos\alpha\sin\eta = \sin\beta. \end{cases} \tag{60}$$

Suppose given $\bar{\eta} \in [-\pi/4, \pi/4]$ fixed and the corresponding iso-η line on any of the six patches covering the cubed-sphere grid. Then the angle $\alpha(\xi)$ corresponding to the point of equiangular coordinates $(\xi, \bar{\eta})$ is

$$\alpha(\xi) = \operatorname{atan}\left(\frac{\tan\xi}{(1+\tan^2\bar{\eta})^{1/2}}\right). \tag{61}$$

Similarly the angle $\beta(\eta)$ corresponding to a point on any iso-ξ line $\xi = \bar{\xi}$ is

$$\beta(\eta) = \operatorname{atan}\left(\frac{\tan\eta}{(1+\tan^2\bar{\xi})^{1/2}}\right). \tag{62}$$

The two identities (61), (62) give on any patch the change of variables $(\xi, \eta) \mapsto (\alpha, \eta)$ and $(\xi, \eta) \mapsto (\xi, \beta)$. Using again the chain rule it is readily verified that

$$\begin{cases} \dfrac{\partial\alpha}{\partial\xi}_{|\eta} = \cos\eta\dfrac{1+\tan^2\xi}{1+\cos^2\eta\tan^2\xi}, \\ \dfrac{\partial\beta}{\partial\eta}_{|\xi} = \cos\xi\dfrac{1+\tan^2\eta}{1+\cos^2\xi\tan^2\eta}. \end{cases} \tag{63}$$

These relations are used in (22). Let us conclude by some remarks on the algebra useful to derive the metric elements on the cubed-sphere grid. If $\boldsymbol{x}(x,y,z)$ denotes a point on the sphere, the covariant vectors g_ξ and g_η are given by [14, 26]:

$$\boldsymbol{g}_\xi = \frac{\partial \boldsymbol{x}}{\partial \xi},\ \boldsymbol{g}_\eta = \frac{\partial \boldsymbol{x}}{\partial \eta}. \tag{64}$$

The metric tensor is

$$G = \begin{bmatrix} \boldsymbol{g}_\xi \cdot \boldsymbol{g}_\xi & \boldsymbol{g}_\xi \cdot g_\eta \\ \boldsymbol{g}_\eta \cdot \boldsymbol{g}_\xi & \boldsymbol{g}_\eta \cdot \boldsymbol{g}_\eta \end{bmatrix} \tag{65}$$

The contravariant vectors are deduced by

$$\begin{cases} \boldsymbol{g}^\xi = G^{11}\boldsymbol{g}_\xi + G^{12}\boldsymbol{g}_\eta, \\ \boldsymbol{g}^\eta = G^{21}\boldsymbol{g}_\xi + G^{22}\boldsymbol{g}_\eta, \end{cases} \tag{66}$$

where

$$G^{-1} = \begin{bmatrix} G^{11} & G^{12} \\ G^{21} & G^{22}. \end{bmatrix} \tag{67}$$

The metric tensor can be expressed using gnomonic coordinates (X,Y) as

$$G = \frac{r^2}{\delta^4}(1+X^2)(1+Y^2)\begin{bmatrix} 1+X^2 & -XY \\ -XY & 1+Y^2 \end{bmatrix}, \tag{68}$$

where $\delta = \sqrt{1+X^2+Y^2}$. The contravariant basis $(\boldsymbol{g}^\xi, \boldsymbol{g}^\eta)$ is given on the patch *Front* (for example) by

$$\boldsymbol{g}^\xi = \frac{1}{x(1+X^2)}\begin{bmatrix} -X \\ 1 \\ 0 \end{bmatrix}, \quad \boldsymbol{g}^\eta = \frac{1}{x(1+Y^2)}\begin{bmatrix} -Y \\ 1 \\ 0 \end{bmatrix}. \tag{69}$$

Similar formulas are obtained for the other patches.

Finally the integral $\mathcal{I}(u)$ over the sphere of radius R of a function $u(\boldsymbol{x})$ is approximated by $\tilde{\mathcal{I}}([u^k_{i,j}])$ defined by

$$\tilde{\mathcal{I}} = \sum_{k=I}^{VI} \tilde{\mathcal{I}}^k. \tag{70}$$

The approximate integral on each patch k is

$$\tilde{\mathcal{I}}^k = R^2 \Delta\xi\Delta\eta \sum_{i,j=-M}^{M}{}' \sqrt{|G^k_{i,j}|}\, u^k_{i,j}, \tag{71}$$

where the prime indicates that the terms corresponding to the $4(N-1)$ interface indices (24) are multiplied by $1/2$ and that the terms corresponding to the four corner indices (25) are multiplied by $1/3$.

References

[1] M. Ben-Artzi, J-P. Croisille, and D. Fishelov. *Navier–Stokes equations in planar domains*. Imperial College Press, ISBN 9781848162754, 2013.

[2] M. Ben-Artzi, J. Falcovitz, and P.G. LeFloch. Hyperbolic conservation laws on the sphere. A geometry compatible finite volume scheme. *J. Comput. Phys.*, 228:5650–5668, 2009.

[3] C. Bogey and C. Bailly. A family of low dispersive and low dissipative explicit schemes for flow noise and noise computations. *J. Comput. Phys.*, 194:194–214, 2003.

[4] L. Collatz. *The Numerical Treatment of Differential Equations*. Springer-Verlag, 3-rd edition, 1960.

[5] P.C. Fragile, C.C. Lindner, P. Anninos, and J.D. Salmonson. Application of the cubed-sphere grid to tilted black-hole accretion disks. *Astrophysical Journal*, 691:482, 2009.
[6] D.V. Gaitonde, J.S. Shang, and J.L. Young. Practical aspects of higher-order numerical schemes for wave propagation phenomena. *Int. J. Numer. Meth. Eng.*, 45:1849–1869, 1999.
[7] C. Hirsch. *Numerical Computation of Internal and External Flows,vol. 1 & 2*. Wiley, 1988.
[8] B.A. Jones, G.H. Born, and G. Beylkin. Comparisons of the cubed-sphere gravity model with the spherical harmonics. *Journal of guidance, control, and dynamics*, 33:415, sqq, 2010.
[9] M.N. Jones. *Spherical Harmonics and Tensors for classical field theory*. Research Studies Press, 1985.
[10] P. Lauritzen, R.D. Nair, and P.A. Ullrich. A conservative semi-lagrangian multi-tracer transport scheme (cslam) on the cubed sphere grid. *J. Comput. Phys.*, 229:1401–1424, 2010.
[11] S. K. Lele. Compact finite-difference schemes with spectral-like resolution. *J. Comput. Phys.*, 103:16–42, 1992.
[12] R.D. Nair, H.-W. Choi, and H.M. Tufo. Computational aspects of a scalable high-order discontinuous Galerkin atmospheric dynamical core. *Comput. Fluids*, 38:309–319, 2009.
[13] R.D. Nair and P. Lauritzen. A class of deformational flow test cases for linear transport problems on the sphere. *J. Comput. Phys.*, 229:8868–8887, 2010.
[14] R.D. Nair, S. Thomas, and R. Loft. A discontinuous Galerkin transport scheme on the cubed sphere. *Month. Weather Review*, 133:814–828, 2005.
[15] N. Paldor and A. Sigalov. An invariant theory of the linearized shallow water equations with rotation. *Dyn. Atmos. Ocean*, 51:26–44, 2010.
[16] W.M. Putman and S-J. Lin. Finite volume transport on various cubed-sphere grids. *J. Comput. Phys.*, 227:55–78, 2007.
[17] S. Redonnet. *Simulation de la propagation acoustique en présence d'écoulements quelconques et de structures solides par résolution numérique des équations d'Euler*. PhD thesis, Univ. Bordeaux 1, 2001.
[18] V. Rokhlin and M. Tygert. Fast algorithms for spherical harmonic expansions. *SIAM J. Sci. Comput.*, 27:1903–1928, 2006.
[19] C. Ronchi, R. Iacono, and P. S. Paolucci. The Cubed Sphere: A new method for the solution of partial differential equations in spherical geometry. *J. Comput. Phys.*, 124:93–114, 1996.
[20] J.A. Rossmanith. A wave propagation method for hyperbolic systems on the sphere. *J. Comput. Phys.*, 213:629–658, 2006.
[21] R. Sadourny. Conservative finite-difference approximations of the primitive equations on quasi-uniform spherical grids. *Mon. Weath. Rev.*, 100:136–144, 1972.
[22] J.-L. Starck, Y. Moudden, P. Abrial, and M. Nguyen. Wavelets, ridgelets and curvelets on the sphere. *Astronomy and Astrophysics*, 2009.
[23] P. N. Swarztrauber, D.L. Williamson, and J.B. Drake. The cartesian method for solving partial differential equations in spherical geometry. *Dynamics of Oceans and Atmospheres*, 27:679–706, 1997.
[24] C.K.W. Tam and J.C. Webb. Dispersion-relation-preserving finite difference schemes for computational acoustics. *J. Comput. Phys.*, 107:262–281, 1993.
[25] S.J. Thomas and R.D. Loft. Semi-implicit spectral element atmospheric model. *J. Sci. Comput.*, 17:339–350, 2002.
[26] P.A. Ullrich, C. Jablonowski, and B. van Leer. High order finite-volume methods for the shallow-water equations on the sphere. *J. Comput. Physics*, 229:6104–6134, 2010.
[27] D.L. Williamson, J.B. Drake, J.J. Hack, R. Jakob, and P. N. Swarztrauber. A standard test set for numerical approximations to the shallow water equations in spherical geometry. *J. Comput. Phys.*, 102:211–224, 1992.

†Université de Lorraine, Département de Mathématiques, F-57045 Metz, France, ‡C.N.R.S., Institut Elie Cartan de Lorraine, UMR 7502, F-57045 Metz, France
E-mail address: jean-pierre.croisille@univ-lorraine.fr